

Article

Structural, Optical and Electrical Properties of HfO₂ Thin Films Deposited at Low-Temperature Using Plasma-Enhanced Atomic Layer Deposition

Kyoung-Mun Kim ^{1,2} , Jin Sub Jang ², Soon-Gil Yoon ¹, Ju-Young Yun ² and Nak-Kwan Chung ^{2,*}

¹ Department of Materials Science and Engineering, Chungnam National University, Daejeon 34134, Korea; kkm1215@kriss.re.kr (K.-M.K.); sgyoon@cnu.ac.kr (S.-G.Y.)

² Department Materials and Energy Measurement Center, Korea Research Institute of Standards and Science (KRISS), Daejeon 34113, Korea; jjs77715@kriss.re.kr (J.S.J.); jyun@kriss.re.kr (J.-Y.Y.)

* Correspondence: nk.chung@kriss.re.kr; Tel.: +82-10-2419-9864

Received: 13 March 2020; Accepted: 23 April 2020; Published: 25 April 2020



Abstract: HfO₂ was deposited at 80–250 °C by plasma-enhanced atomic layer deposition (PEALD), and properties were compared with those obtained by using thermal atomic layer deposition (thermal ALD). The ALD window, i.e., the region where the growth per cycle (GPC) is constant, shifted from high temperatures (150–200 °C) to lower temperatures (80–150 °C) in PEALD. HfO₂ deposited at 80 °C by PEALD showed higher density (8.1 g/cm³) than those deposited by thermal ALD (5.3 g/cm³) and a smooth surface (RMS Roughness: 0.2 nm). HfO₂ deposited at a low temperature by PEALD showed decreased contaminants compared to thermal ALD deposited HfO₂. Values of refractive indices and optical band gap of HfO₂ deposited at 80 °C by PEALD (1.9, 5.6 eV) were higher than those obtained by using thermal ALD (1.7, 5.1 eV). Transparency of HfO₂ deposited at 80 °C by PEALD on polyethylene terephthalate (PET) was high (> 84%). PET deposited above 80 °C was unable to withstand heat and showed deformation. HfO₂ deposited at 80 °C by PEALD showed decreased leakage current from 1.4×10^{-2} to 2.5×10^{-5} A/cm² and increased capacitance of approximately 21% compared to HfO₂ using thermal ALD. Consequently, HfO₂ deposited at a low temperature by PEALD showed improved properties compared to HfO₂ deposited by thermal ALD.

Keywords: HfO₂ thin film; low temperature; plasma-enhanced atomic layer deposition; electrical properties

1. Introduction

The semiconductor industry has developed rapidly, and electronic devices have been scaled down. However, scaled-down devices can show many problems, such as direct tunneling, high gate leakage current and poor reliability [1,2]. Therefore, HfO₂ has been studied to replace conventional SiO₂ as a high- κ material because of its advantages, such as high density, good ductility and corrosion resistance, as well as its high-k [3,4]. HfO₂ has mainly been deposited by thermal atomic layer deposition (thermal ALD) because this method produces thin films that are pinhole-free, high density and have low contaminants levels (Carbon, Nitrogen); this process also allows excellent thickness control [5–8].

Recently, as the importance of wearable devices has increased, low-temperature deposition of HfO₂ thin films has been required [9,10]. However, HfO₂ thin films normally must be deposited at around 200 °C because the metal–organic precursors used as sources during the ALD process fully decompose at high temperatures [11]. Many methods have been studied to lower the deposition temperature of HfO₂ in ALD [12–16]. However, in those studies, HfO₂ thin films deposited at low temperatures had problems, such as a high level of carbon impurities (5.15%–8.9% carbon impurity in HfO₂ thin films

deposited at 150 °C) or low density (3.7 g/cm³ when deposited at 30 °C, 4.1 g/cm³ at 50 °C, 4.8 g/cm³ at 80 °C and 5.3 g/cm³ at 100 °C); these problems cause high leakage current and poor reliability in electronic devices [12–14].

Using plasma to produce oxygen radicals with high reactivity can solve these problems, and plasma has been used in other low-temperature deposition processes [17]. Consequently, plasma-enhanced atomic layer deposition (PEALD) can be used to decompose a source at a lower temperature by making atomic oxygen radicals using O₂ gas as a reactant; this is in contrast to the conventional thermal ALD process, which uses O₃ as a reactant. In the previous studies, it was found that the electrochemical oxidation potential, a measure of the sensitivity of the oxidation reaction, of atomic oxygen radicals (2.42 V) is higher than that of O₃ (2.08 V) [18–20]. In the ALD process, electrochemical oxidation potential of the reactants indicates the ligand-decomposing power [21–24]. Higher oxidation potential of reactants enables the low-temperature processes because less thermal energy is required for source decomposition [16].

In this study, HfO₂ thin films were deposited by PEALD at 80 °C, and their variable properties, such as film structures, surface morphology and surface components, were compared with thin films deposited by using thermal ALD and PEALD at various temperatures (80, 150 and 250 °C). Moreover, values of densities, refractive index, optical bandgap determined by Tauc plot and transmittance of HfO₂ deposited at 80 °C by thermal ALD and PEALD were compared. In our study, the HfO₂ deposited at a low temperature (80 °C) by PEALD showed a low carbon ratio (3.5%) and high film density (8.1 g/cm³). Finally, electrical characteristics, such as capacitance–voltage (C–V) curve, current–voltage (I–V) and fixed-charge density (Q_f) of HfO₂ deposited at 80, 150 and 250 °C were analyzed, using an MOS capacitor. The HfO₂ thin films deposited at a low temperature (80 °C), using PEALD, showed improved structural, chemical, optical and electrical properties, without any degradation.

2. Materials and Methods

Using an automated ALD system (iCV d300, ISAC Research, Daejeon, Korea), HfO₂ thin films were fabricated on doped ($\rho \sim 15 \Omega \cdot \text{cm}$) p-type Si (100) wafers. Substrates were cleaned for 10 min with acetone, 10 min with ethanol and 10 min with IPA in an ultrasonic generator; they were immediately dried by blowing argon over the sample. The substrates were loaded at different temperatures, in a range of 80–250 °C. The main pump was an MVP-90 (WOOSUNG VACUUM PUMP, Jeju, Korea), and the base pressure was 10 mtorr. An ISP-90 (ANEST IWATA Corporation, Yokohama, Japan) was used as a by-pass pump for constant flow. In this experiment, direct plasma was used; the plasma power was fixed at 150 W, using a 13.56 MHz RF power supply (REX2-3K, RF Power Tech, Anyang, Korea). Tetrakis(ethylmethylamino) hafnium (TEMAH-99.999% purity from UP Chemical, Pyungtaek, Korea) was used as a precursor. High-purity O₃ and O₂ were used as oxidants. O₃ was produced from O₂ by an ozone generator (LAB-II, Ozonotech, Daejeon, Korea). Ar gas, used as a carrier gas and purge gas, also had a purity of 99.999%. TEMAH precursor canister was maintained at 75 °C. The precursor flow line and the chamber were also maintained at 80 °C, to prevent condensation and clogging.

The thickness of the HfO₂ thin films was measured by using a Reflectometer (ST2000, K-MAC, Daejeon, Korea) and Spectroscopic Ellipsometry (SE, M2000D, J.A. WOOLLAM CO, Lincoln, NE, USA). In addition, the film structures and density in HfO₂ were examined by Grazing Incidence X-ray diffraction and X-ray reflectivity, respectively (GIXRD, MXD10, Rigaku, Tokyo, Japan, Cu K α radiation). The root mean square (RMS) roughness values of the HfO₂ films (50 nm) were obtained by Atomic Force Microscope (AFM, XE7, Park Systems Suwon, Korea) images and scanned at 2 $\mu\text{m} \times 2 \mu\text{m}$ size. The chemical bonding states and components were examined by using X-ray photoelectron spectroscopy (XPS, K-Alpha+, Thermo Fisher Scientific Waltham, MA, USA) To remove carbon- and nitrogen-contaminant layers from air, approximately 7 to 10 nm of the HfO₂ films was removed via Ar etching, at 1 keV, for 30 s [25,26]. Refractive index and absorption coefficient of HfO₂ (50 nm) were extracted from the Ellipsometry (SE, M2000D, J.A. WOOLLAM CO, Lincoln, NE, USA) data. The transmittance of HfO₂ (50 nm) at 550 nm on the PET substrate (ST510, DuPont Teijin Films, Wilmington, DE, USA) was measured in a range

from 190 to 1100 nm, which was measured in the normal incidence of light by UV-vis spectroscopy (HP 8453, Agilent, Santa Clara, CA, USA). To measure the electrical properties (I–V and C–V), MOS capacitors were fabricated. Cu/Ti top electrodes were deposited on HfO₂/p-Si, using an E-beam evaporator (KVET—C500200, Korea Vacuum, Gimpo, Korea). Cu/Ti circular electrodes were patterned, using a shadow mask. Electrical properties, as indicated by the I–V and C–V curves, were measured by using a Manual Probe Station (SUMMIT 11862B, Cascade, Beaverton, OR, USA). The C–V curve was obtained at 1 MHz in the range of –7 to +7 V, and the I–V curve was obtained from –2 to 2 V.

3. Results and Discussion

To show the experimental conditions of HfO₂ thin films deposited at 80 °C, Figure 1a–d provides growth per cycle (GPC) curves for each step time; these were measured by using a reflectometer, because the process is easier and simpler than ellipsometry.

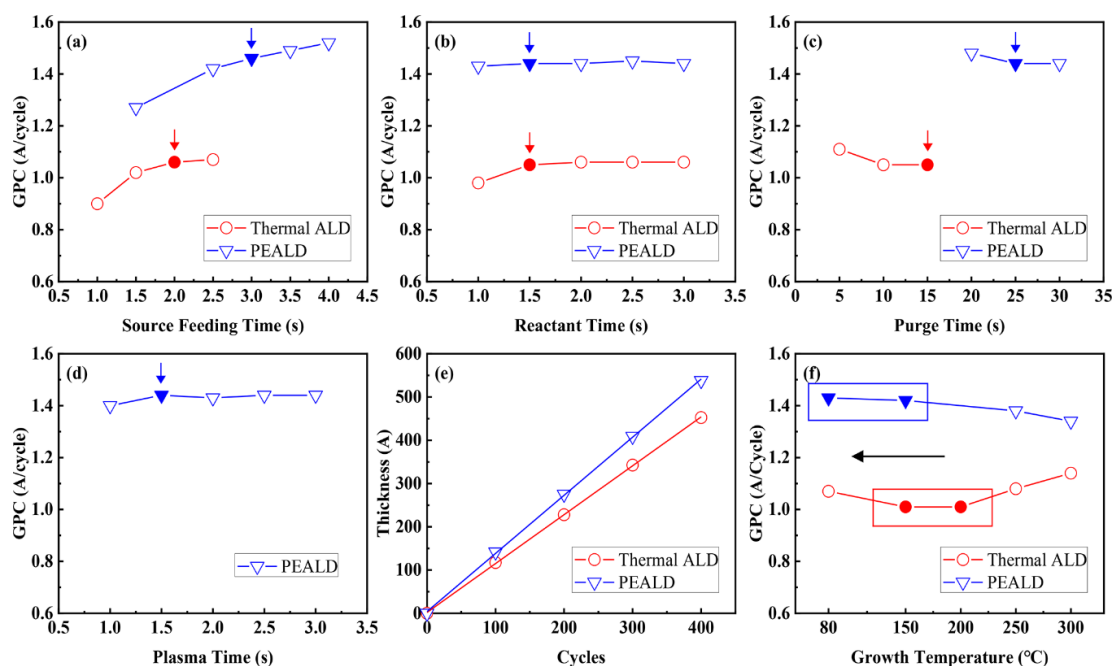


Figure 1. (a–d) GPC values of HfO₂ deposited at 80 °C by thermal ALD and PEALD as functions of precursor exposure time, reactant exposure time, purge time and plasma exposure time. (e) Thickness values as a function of ALD cycles with thermal ALD and PEALD. (f) ALD windows as functions of deposition temperature with thermal ALD (150–200 °C) and PEALD (80–150 °C).

GPC curves, which changed according to the feeding and purge times, were clearly saturated at the same time with sufficient feeding and purge times. The experimental periods were determined according to these saturation times, as indicated by the arrows in Figure 1a–d. The thermal ALD cycle for HfO₂ deposition consisted of 2 s source feeding, 15 s Ar purging, 1.5 s O₃ reactant feeding and 15 s Ar purging. Additionally, the PEALD cycle for HfO₂ deposition consisted of 3 s source feeding, 25 s Ar purging, 1.5 s O₂ reactant feeding, a 1.5 s O₂ plasma-on state and 25 s Ar purging. Since direct plasma was used in the experiment, O₂ plasma was used for a relatively short time compared with remote plasma. Figure 1e shows the thickness increase with the deposition cycle; resulting values were obtained by ellipsometry, to measure the thicknesses of the thin films, because the reflectometer has difficulty accurately measuring thicknesses under 100 nm. The HfO₂ thickness increased linearly as the cycle increased, without a growth delay problem; GPC values were similar to those obtained from using the reflectometer.

Figure 1f shows the GPC of HfO₂ thin film according to the deposition temperatures of the thermal ALD and PEALD processes. The temperature section in which GPC shows constant temperature is

called the ALD window and is a problem-free deposition region. The region between 150 and 200 °C is the ALD window in thermal ALD. In PEALD, the ALD window shifted to lower temperatures (80–150 °C) from high temperatures (150–200 °C) because of the high reactivity of O₂ plasma; this allowed more stable low-temperature deposition. When thin films were deposited at 80 °C, using thermal ALD, GPC increased and exhibited condensation because of the insufficient thermal energy. Above 250 °C in thermal ALD, because of source decomposition due to high thermal energy, the GPC increased as the temperature increased. Conversely, in PEALD, GPC decreased, and desorption occurred in a manner different from that in thermal ALD [27]. The reason for this is that, as the temperature rose, increased ion energy of the plasma promoted etching of the HfO₂ thin film and caused desorption [28].

Figure 2a,b shows the XRD pattern of HfO₂ when deposited by thermal ALD and PEALD [29].

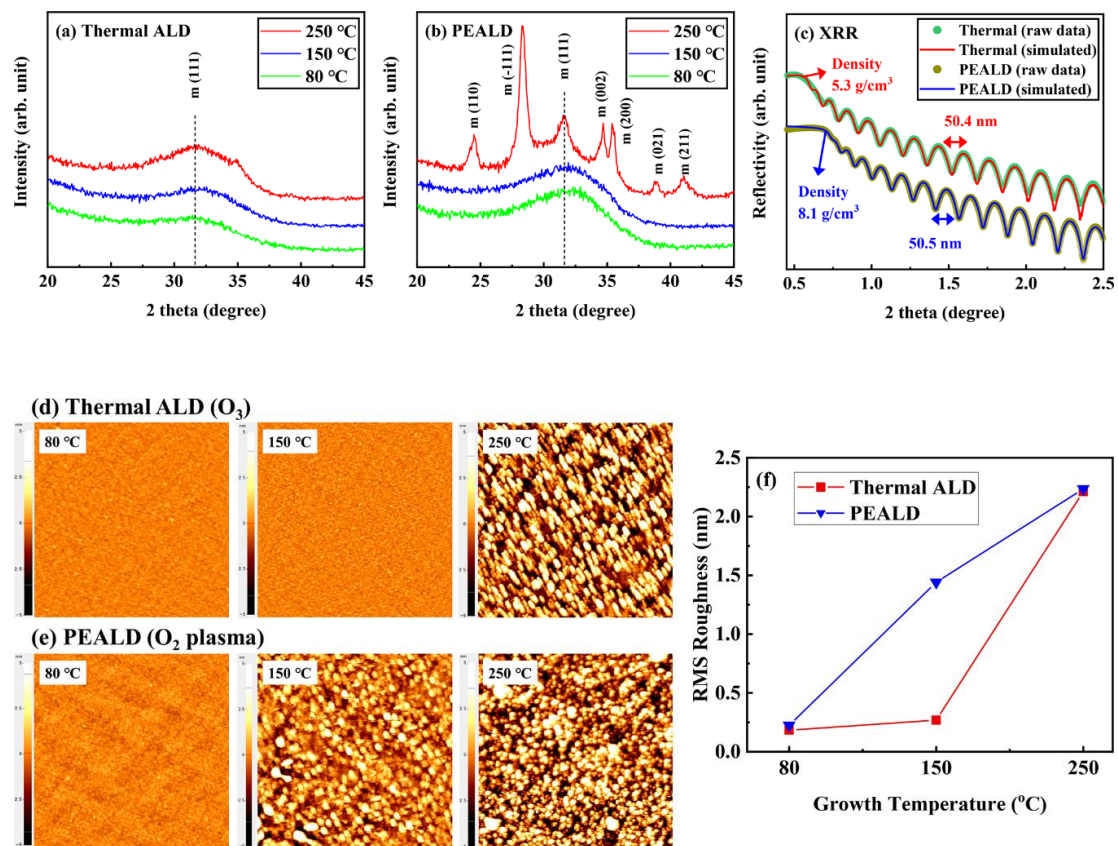


Figure 2. (a,b) XRD pattern in HfO₂ thin films (50 nm) deposited at 80–250 °C by thermal ALD and PEALD, measured by GIXRD. (c) Density of HfO₂ thin films (50 nm) formed at 80 °C by thermal ALD and PEALD, measured by XRR. (d,e) AFM topography images of HfO₂ thin films (50 nm) deposited by thermal ALD and PEALD. (f) Root mean square (RMS) roughness of HfO₂ by growth temperatures (80–250 °C).

XRD patterns of HfO₂ deposited at 80–250 °C by thermal ALD showed a broad peak at $2\theta = 32^\circ$, indicating a dominantly amorphous structure HfO₂ thin film [30]. Moreover, HfO₂ deposited at 80–150 °C by PEALD also had an amorphous structure, but HfO₂ deposited at 250 °C by PEALD contained a polycrystalline structure. This means that the crystallization of HfO₂ thin film deposited by PEALD started at a lower temperature than that of HfO₂ deposited by thermal ALD [31]. Figure 2c shows the thickness and density of HfO₂ deposited at 80 °C, obtained from a period and critical angle of reflectivity oscillation pattern, as measured by XRR. Thickness was measured and found to be approximately 50 nm for both thermal ALD and PEALD samples, and density increased in PEALD from 5.3 to 8.1 g/cm³. This means that the HfO₂ thin film deposited by PEALD at a low temperature was

denser than that deposited to the same thickness by thermal ALD. Figure 2d–f provides root mean square (RMS) roughness and morphology images of HfO_2 deposited according to temperature (80–250 °C) in thermal ALD and PEALD. In the PEALD samples, there was no difference of roughness compared to the thermal ALD samples, and the HfO_2 thin film was still flat at 80 °C (0.2 nm). Additionally, no large particles were seen when HfO_2 was deposited at a low temperature. As the temperature rose, the roughness of the thin film rapidly increased due to the formation of crystallite [32].

Figure 3a,b shows XPS results for Hf 4f formed by thermal ALD and PEALD, respectively.

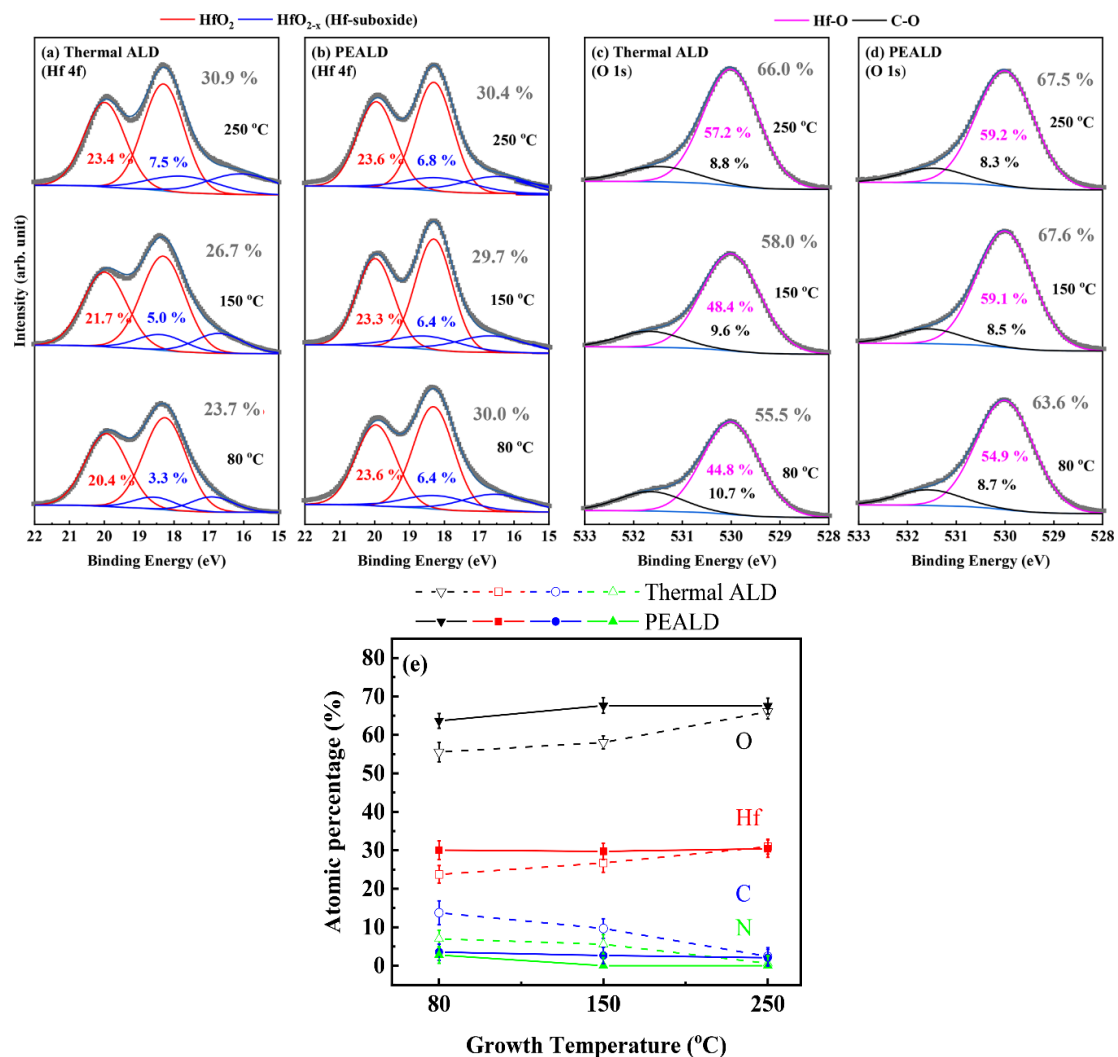


Figure 3. (a,b) Hf 4f and (c,d) O 1s spectra of HfO_2 thin films (50 nm) on Si substrate fabricated by thermal ALD and PEALD. Gray dotted lines and blue solid lines are sum of the spectra before fitting and sum of the deconvoluted peaks after fitting, respectively. (e) Surface component percentages of O, Hf, C and N in HfO_2 thin films (50 nm). The error bars represent the standard deviations.

The deconvoluted Hf 4f spectra show the doublet of peaks at binding energy of 18.31 and 19.99 eV, which is associated with HfO_2 [33]. Moreover, at binding energy lower than those of the 4f doublet, the suboxide peaks are located at 16.93 and 18.63 eV, and they are associated with HfO_{2-x} . The atomic concentration of hafnium in HfO_2 thin film deposited at a low temperature by thermal ALD was the lowest at 23.7%, because many defects, such as carbon, nitrogen and hydroxyl groups ($-\text{OH}$), were located in the HfO_2 thin films. Conversely, the atomic concentration of hafnium in HfO_2 deposited at 80 °C by PEALD was high, at 30.0%, due to the low level of contaminants, similar to the sample deposited at 250 °C by thermal ALD. Figure 3c,d shows the XPS results for O 1s after thermal ALD and

PEALD. O 1s peaks are deconvoluted into two components, a signal associated with HfO₂ at 530.03 eV and an additional peak associated with carbon and oxygen at 531.68 eV [33]. The C–O peaks represent impurity carbon defects combined with oxygen, which can reduce the performance and efficiency of electronic devices [34,35]. According to these results, as the deposition temperature increased from 80 to 250 °C in both the thermal ALD and PEALD processes, the ratio of the C–O peaks showed a tendency to decrease. Furthermore, in the PEALD process, the ratio of C–O peaks was reduced compared with thermal ALD at all temperatures. In particular, at 80 °C in PEALD, C–O peaks decreased more than at 250 °C in thermal ALD. The atomic concentration of oxygen in HfO₂ was similar, except for the thin film deposited at a low temperature by thermal ALD. As mentioned previously for elemental Hf, the presence of many contaminants can lower the atomic concentration of oxygen in thin films.

Figure 3e shows surface component percentages of O, Hf, C and N in the HfO₂ thin films. Carbon and nitrogen inside the film act as defects, causing a decrease of density or degradation of properties. At a low temperature, HfO₂ deposited through thermal ALD had high ratios of carbon (13.8%) and nitrogen (7.0%) because of incomplete source decomposition. Conversely, in the case of thin films deposited through PEALD, both carbon (3.5%) and nitrogen (2.8%) ratios were low, even at low temperatures. This suggests that, in PEALD, because the precursor was decomposed more by O₂ plasma than by O₃, the number of inner defects was lower than in thermal ALD at a low temperature.

Figure 4a shows refractive index (n) and extinction coefficient (k) as a function of the photon energy (eV) of HfO₂ films (50 nm) deposited at 80 °C.

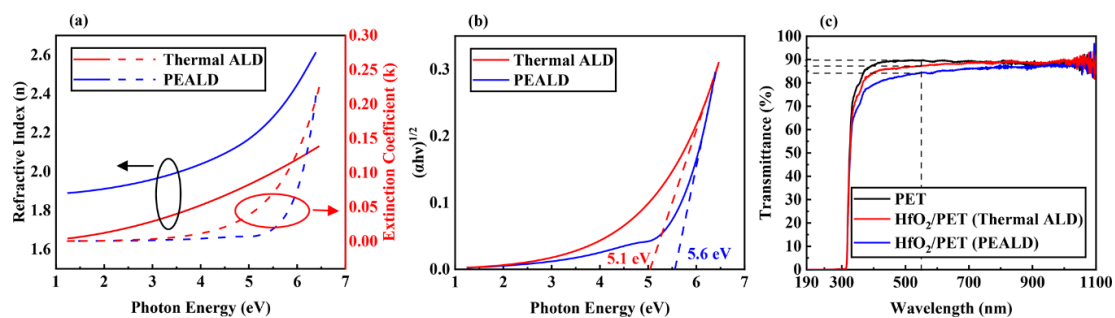


Figure 4. (a) Refractive index (n), extinction coefficient (k) and (b) optical bandgap values extracted using the Tauc method for HfO₂ films (50 nm) formed at 80 °C, using thermal ALD and PEALD, as measured by ellipsometry. (c) Transmittance of HfO₂ thin films (50 nm) deposited at 80 °C by thermal ALD and PEALD on PET substrate.

Using ellipsometry, values of n and k were calculated from the real and imaginary parts of the complex dielectric function ($\epsilon = \epsilon_1 + i\epsilon_2$), respectively [36]. The n values of the HfO₂ are associated with the density of HfO₂ thin films [37,38]. Since the HfO₂ film deposited by PEALD had less carbon content and a lower O/Hf ratio than that obtained from using thermal ALD, it is expected that the HfO₂ film deposited by PEALD has a higher density than that deposited by using thermal ALD. Therefore, the n value of the HfO₂ deposited with PEALD was higher than that of HfO₂ deposited with thermal ALD in all photon energy ranges. Figure 4b shows optical-band-gap values obtained from using the absorption coefficient ($\alpha = 4\pi k/\lambda$) of HfO₂ thin films (50 nm) deposited at 80 °C. The band gap of HfO₂ thin film in the previous studies were typically between 5.6 and 5.7 eV [39,40]. However, the band gap of HfO₂ deposited by thermal ALD was lower at 5.1 eV. When HfO₂ was deposited by PEALD, the optical band gap increased to 5.6 eV. If the optical band gap is small, HfO₂ thin films cannot function properly as insulators. Optical band gap was plotted by using the Tauc method, as described in Equation (1) [41]:

$$(ah\nu)^{1/2} = A(h\nu - E_g) \quad (1)$$

where $\alpha(= 4\pi k/\lambda)$ is the absorption coefficient, h is Planck's constant, ν is photon frequency, A is a proportionality constant and E_g is the optical band gap.

Figure 4c shows the transmittance of HfO₂ (50 nm) deposited at 80 °C on PET substrate. The transmittance of HfO₂ deposited by PEALD was high (>84%) in the visible region (89.7% for bare PET substrate, 87.2% after thermal ALD and 84.3% for PEALD at wavelength of 550 nm). The transmittance decreased slightly for PEALD compared to thermal ALD because the HfO₂ film deposited by PEALD was denser [42]. When HfO₂ was deposited at more than 80 °C on PET substrate, PET could not endure the heat, and deformation occurred.

Figure 5a,b shows C–V curves of HfO₂ deposited by thermal ALD and PEALD, respectively.

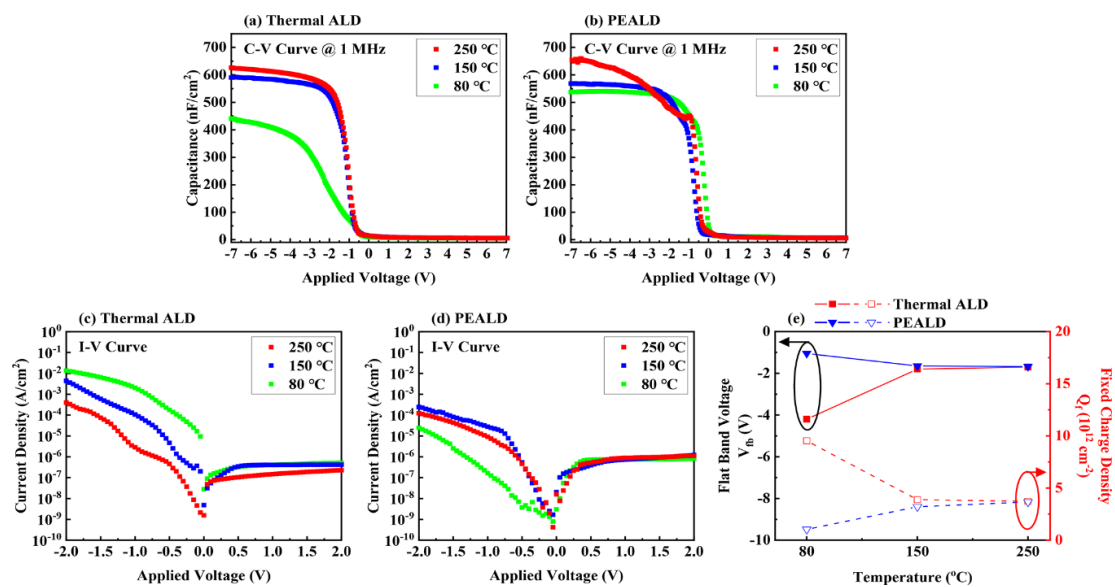


Figure 5. (a,b) C–V and (c,d) I–V curves of HfO₂ (10 nm) MOS capacitors fabricated, using thermal ALD and PEALD. (e) Flat band voltage and fixed charge density of HfO₂ (10 nm) MOS capacitor according to growth temperature (80–250 °C).

Capacitance of HfO₂ deposited at 80 °C by PEALD increased from 444.9 to 540.1 nF/cm², an approximately 21% increase. The dielectric constant (κ -value) of HfO₂ deposited at 80 °C in PEALD (12.6) was higher than those of samples deposited by thermal ALD (8.7). Since the native oxide was not etched on the Si substrate, the κ -value was calculated by considering the native oxide thickness (~3 nm) [43,44]. Moreover, the κ -value of HfO₂ thin film was calculated from the value of C_{HfO_2} , using the following formula, Equation (2):

$$\frac{1}{C_{\text{HfO}_2}} = \frac{1}{C_{\text{ox}}} - \frac{1}{C_{\text{SiO}_2}} \quad (2)$$

where C_{HfO_2} and C_{SiO_2} are the capacitance of HfO₂ and SiO₂, respectively. C_{ox} is the overall capacitance of the MOS capacitor.

There was no significant improvement at temperatures other than 80 °C. Figure 5c,d shows I–V curves of HfO₂ deposited by thermal ALD and PEALD. Leakage currents at negative voltage in PEALD were reduced overall compared to those for thermal ALD. Significantly, at 80 °C, the leakage current decreased from 1.4×10^{-2} A/cm² to 2.5×10^{-5} A/cm² at –2 V, which was lower than that of HfO₂ deposited at 250 °C by thermal ALD. Because HfO₂ films deposited by PEALD at a low temperature were denser, contaminants in the thin films were reduced [45]. Because we used an NMOS capacitor with a p-type Si substrate, a depletion layer formed at the interface when the voltage was positive. For this sample, almost no current flowed, because the capacitor was in an inversion state.

Figure 5e shows the flat band voltage (V_{fb}) and fixed charge density (Q_f), extracted from the C–V curves in Figure 5a,b. V_{fb} of HfO₂ deposited by PEALD at 80 °C was lower than those of sample formed by thermal ALD. Q_f of HfO₂ deposited at 80 °C by PEALD decreased about 90%, from 9.5×10^{12} to 1.0×10^{12} , the lowest value in all temperature ranges (80–250 °C). V_{fb} and Q_f showed almost

identical values at all temperatures, except 80 °C. Q_f has a (+) charge and is distributed at the interface between Si and the HfO₂ thin film, which puts the device into a (+) state and makes it to work at higher voltage. This suggests that, at low temperatures of around 80 °C, capacitors using HfO₂ deposited by PEALD will have better electrical properties than those using HfO₂ deposited by thermal ALD. However, the Q_f value of HfO₂ deposited by PEALD tended to increase as the temperature increased. This means that, as the deposition temperature rose, the substrate was damaged by increased plasma ion energy during deposition [46,47].

4. Conclusions

In this study, HfO₂ thin films deposited at a low temperature (80 °C), using PEALD with O₂ plasma, showed improved properties compared to films deposited by using thermal ALD. The ALD window shifted from high temperatures (150–200 °C) to low temperatures (80–150 °C) when using PEALD, allowing stable deposition at a low temperature. HfO₂ deposited by low-temperature PEALD showed a flat surface and higher density than films deposited by thermal ALD. Moreover, HfO₂ deposited at 80 °C by PEALD showed a decreased presence of contaminants, such as carbon and nitrogen, compared to films deposited by thermal ALD. HfO₂ thin films deposited by PEALD showed an increased refractive index, improved optical band gap (5.6 eV) and high transparency of ~84%. Denser and lower-contaminant HfO₂ thin films deposited by PEALD contributed to capacitance improvement of about 21%, low leakage current of 2.5×10^{-5} A/cm² and the lowest fixed charge density (1.0×10^{12}). As a result, due to the higher decomposition power of O₂ plasma, HfO₂ thin films deposited at a low temperature by PEALD showed improved properties compared to those of films deposited by thermal ALD.

Author Contributions: K.-M.K. and J.S.J. performed the experiments; K.-M.K. and N.-K.C. analyzed the data; S.-G.Y. and N.-K.C. contributed material and experimental tools; K.-M.K., J.-Y.Y. and N.-K.C. wrote the paper. All authors have read and agreed to the published version of the manuscript.

Funding: This research was supported by Characterization Platform for Advanced Materials and Development of Reliability Measurement Technology for Hydrogen Refueling Station funded by Korea Research Institute of Standards and Science (KRISS-2020-GP2020-0011, KRISS-2020-GP2020-0007).

Conflicts of Interest: The authors declare no competing financial interests.

References

1. Masuda, H.; Nakai, M.; Kubo, M. Characteristics and limitation of scaled-down MOSFET's due to two-dimensional field effect. *IEEE Trans. Electron Devices* **1979**, *26*, 980–986. [[CrossRef](#)]
2. Han, D.; Kang, J.; Lin, C.; Han, R. Reliability characteristics of high-K gate dielectrics HfO₂ in metal-oxide semiconductor capacitors. *Microelectron. Eng.* **2003**, *66*, 643–647. [[CrossRef](#)]
3. Gusev, E.P.; D'Emic, C.P. Charge detrapping in HfO₂ high-κ gate dielectric stacks. *Appl. Phys. Lett.* **2003**, *83*, 5223–5225. [[CrossRef](#)]
4. Nakajima, K.; Joumori, S.; Suzuki, M.; Kimura, K.; Osipowicz, T.; Tok, K.L.; Zheng, J.Z.; See, A.; Zhang, B.C. Strain profiling of HfO₂/Si(001) interface with high-resolution Rutherford backscattering spectroscopy. *Appl. Phys. Lett.* **2003**, *83*, 296–298. [[CrossRef](#)]
5. An, J.-K.; Chung, N.-K.; Kim, J.-T.; Hahm, S.-H.; Lee, G.; Lee, S.; Lee, T.; Park, I.-S.; Yun, J.-Y. Effect of Growth Temperature on the Structural and Electrical Properties of ZrO₂ Films Fabricated by Atomic Layer Deposition Using a CpZr[N(CH₃)₂]₃/C₇H₈ Cocktail Precursor. *Materials* **2018**, *11*, 386. [[CrossRef](#)] [[PubMed](#)]
6. He, W. ALD: Atomic Layer Deposition—Precise and Conformal Coating for Better Performance. In *Handbook of Manufacturing Engineering and Technology*; Springer: London, UK, 2015; pp. 2959–2996, ISBN 9781447146704.
7. Johnson, R.W.; Hultqvist, A.; Bent, S.F. A brief review of atomic layer deposition: From fundamentals to applications. *Mater. Today* **2014**, *17*, 236–246. [[CrossRef](#)]
8. Vähä-Nissi, M.; Pitkänen, M.; Salo, E.; Sievänen-Rahijärvi, J.; Putkonen, M.; Harlin, A. Atomic layer deposited thin barrier films for packaging. *Cellul. Chem. Technol.* **2015**, *49*, 575–585.
9. Zou, M.; Ma, Y.; Yuan, X.; Hu, Y.; Liu, J.; Jin, Z. Flexible devices: From materials, architectures to applications. *J. Semicond.* **2018**, *39*, 011010. [[CrossRef](#)]

10. Huang, S.; Liu, Y.; Zhao, Y.; Ren, Z.; Guo, C.F. Flexible Electronics: Stretchable Electrodes and Their Future. *Adv. Funct. Mater.* **2019**, *29*, 1805924. [[CrossRef](#)]
11. Oh, N.K.; Kim, J.-T.; Ahn, J.-K.; Kang, G.; Kim, S.Y.; Yun, J.-Y. The Effects of Thermal Decomposition of Tetrakis-ethylmethylaminohafnium (TEMAHf) Precursors on HfO₂ Film Growth using Atomic Layer Deposition. *Appl. Sci. Conver. Technol.* **2016**, *25*, 56–60. [[CrossRef](#)]
12. Niu, G.; Kim, H.-D.; Roelofs, R.; Perez, E.; Schubert, M.A.; Zaumseil, P.; Costina, I.; Wenger, C. Material insights of HfO₂-based integrated 1-transistor-1-resistor resistive random access memory devices processed by batch atomic layer deposition. *Sci. Rep.* **2016**, *6*, 28155. [[CrossRef](#)] [[PubMed](#)]
13. Fan, J.; Liu, H.; Kuang, Q.; Gao, B.; Ma, F.; Hao, Y. Physical properties and electrical characteristics of H₂O-based and O₃-based HfO₂ films deposited by ALD. *Microelectron. Reliab.* **2012**, *52*, 1043–1049. [[CrossRef](#)]
14. Kim, J.H.; Park, T.J.; Kim, S.K.; Cho, D.-Y.; Jung, H.-S.; Lee, S.Y.; Hwang, C.S. Chemical structures and electrical properties of atomic layer deposited HfO₂ thin films grown at an extremely low temperature (≤ 100 °C) using O₃ as an oxygen source. *Appl. Surf. Sci.* **2014**, *292*, 852–856. [[CrossRef](#)]
15. Richter, C.; Schenk, T.; Schroeder, U.; Mikolajick, T. Film properties of low temperature HfO₂ grown with H₂O, O₃, or remote O₂-plasma. *J. Vac. Sci. Technol. A Vac. Surf. Film.* **2014**, *32*, 01A117. [[CrossRef](#)]
16. Xiao, Z.; Kisslinger, K.; Chance, S.; Banks, S. Comparison of Hafnium Dioxide and Zirconium Dioxide Grown by Plasma-Enhanced Atomic Layer Deposition for the Application of Electronic Materials. *Crystals* **2020**, *10*, 136. [[CrossRef](#)]
17. Chen, Z.; Wang, H.; Wang, X.; Chen, P.; Liu, Y.; Zhao, H.; Zhao, Y.; Duan, Y. Low-temperature remote plasma enhanced atomic layer deposition of ZrO₂/zirconia nanolaminate film for efficient encapsulation of flexible organic light-emitting diodes. *Sci. Rep.* **2017**, *7*, 1–9. [[CrossRef](#)]
18. Barrera-Díaz, C.; Cañizares, P.; Fernández, F.J.; Natividad, R.; Rodrigo, M.A. Electrochemical Advanced Oxidation Processes: An Overview of the Current Applications to Actual Industrial Effluents. *J. Mex. Chem. Soc.* **2017**, *58*, 256–275. [[CrossRef](#)]
19. Poyatos, J.M.; Muñoz, M.M.; Almecija, M.C.; Torres, J.C.; Hontoria, E.; Osorio, F. Advanced Oxidation Processes for Wastewater Treatment: State of the Art. *Water. Air. Soil Pollut.* **2010**, *205*, 187–204. [[CrossRef](#)]
20. Rodríguez, A.; Rosal, R.; Perdígón-Melón, J.A.; Mezcuca, M.; Agüera, A.; Hernando, M.D.; Letón, P.; Fernández-Alba, A.R.; García-Calvo, E. Ozone-Based Technologies in Water and Wastewater Treatment. In *Emerging Contaminants from Industrial and Municipal Waste*; Springer: Berlin/Heidelberg, Germany, 2008; pp. 127–175, ISBN 9783540792093.
21. Profijt, H.B.; Potts, S.E.; van de Sanden, M.C.M.; Kessels, W.M.M. Plasma-Assisted Atomic Layer Deposition: Basics, Opportunities, and Challenges. *J. Vac. Sci. Technol. A Vac. Surf. Film.* **2011**, *29*, 050801. [[CrossRef](#)]
22. Provine, J.; Schindler, P.; Torgersen, J.; Kim, H.J.; Karthaler, H.-P.; Prinz, F.B. Atomic layer deposition by reaction of molecular oxygen with tetrakisdimethylamido-metal precursors. *J. Vac. Sci. Technol. A Vac. Surf. Film.* **2016**, *34*, 01A138. [[CrossRef](#)]
23. Fang, G.Y.; Xu, L.N.; Cao, Y.Q.; Wang, L.G.; Wu, D.; Li, A.D. Self-catalysis by aminosilanes and strong surface oxidation by O₂ plasma in plasma-enhanced atomic layer deposition of high-quality SiO₂. *Chem. Commun.* **2015**, *51*, 1341–1344. [[CrossRef](#)] [[PubMed](#)]
24. Becker, M.; Sierka, M. Atomistic simulations of plasma-enhanced atomic layer deposition. *Materials* **2019**, *12*, 2605. [[CrossRef](#)] [[PubMed](#)]
25. Hoflund, G.B. Application of novel O- and H-atom sources in molecular beam epitaxy. *J. Vac. Sci. Technol. B Microelectron. Nanom. Struct.* **1998**, *16*, 1446. [[CrossRef](#)]
26. Khanuja, M.; Sharma, H.; Mehta, B.R.; Shivaprasad, S.M. XPS depth-profile of the suboxide distribution at the native oxide/Ta interface. *J. Electron Spectros. Relat. Phenom.* **2009**, *169*, 41–45. [[CrossRef](#)]
27. Knoop, H.C.M.; Potts, S.E.; Bol, A.A.; Kessels, W.M.M. Atomic Layer Deposition. In *Handbook of Crystal Growth*; Elsevier: Amsterdam, The Netherlands, 2015; pp. 1101–1134, ISBN 9780444633040.
28. Chae, H.; Sawin, H.H. Plasma Kinetic Study of Silicon-Dioxide Removal with Fluorocompounds in a Plasma-Enhanced Chemical Vapor Deposition Chamber. *J. Korean Phys. Soc.* **2007**, *51*, 978. [[CrossRef](#)]
29. Cho, D.-Y.; Jung, H.S.; Yu, I.-H.; Yoon, J.H.; Kim, H.K.; Lee, S.Y.; Jeon, S.H.; Han, S.; Kim, J.H.; Park, T.J.; et al. Stabilization of Tetragonal HfO₂ under Low Active Oxygen Source Environment in Atomic Layer Deposition. *Chem. Mater.* **2012**, *24*, 3534–3543. [[CrossRef](#)]
30. Kondaiah, P.; Shaik, H.; Mohan Rao, G. Studies on RF magnetron sputtered HfO₂ thin films for microelectronic applications. *Electron. Mater. Lett.* **2015**, *11*, 592–600. [[CrossRef](#)]

31. Luo, X.; Li, Y.; Yang, H.; Liang, Y.; He, K.; Sun, W.; Lin, H.-H.; Yao, S.; Lu, X.; Wan, L.; et al. Investigation of HfO₂ Thin Films on Si by X-ray Photoelectron Spectroscopy, Rutherford Backscattering, Grazing Incidence X-ray Diffraction and Variable Angle Spectroscopic Ellipsometry. *Crystals* **2018**, *8*, 248. [CrossRef]
32. Blaschke, D.; Munnik, F.; Grenzer, J.; Rebohle, L.; Schmidt, H.; Zahn, P.; Gemming, S. A correlation study of layer growth rate, thickness uniformity, stoichiometry, and hydrogen impurity level in HfO₂ thin films grown by ALD between 100 °C and 350 °C. *Appl. Surf. Sci.* **2020**, *506*, 144188. [CrossRef]
33. Chourasia, A.R.; Hickman, J.L.; Miller, R.L.; Nixon, G.A.; Seabolt, M.A. X-Ray Photoemission Study of the Oxidation of Hafnium. *Int. J. Spectrosc.* **2009**, *2009*, 1–6. [CrossRef]
34. Sopori, B.; Rupnowski, P.; Shet, S.; Budhraj, V.; Call, N.; Johnston, S.; Seacrist, M.; Shi, G.; Chen, J.; Deshpande, A. Influence of defects and defect distributions in multicrystalline silicon on solar cell performance. In Proceedings of the 35th IEEE Photovoltaic Specialists Conference, Honolulu, HI, USA, 20–25 June 2010.
35. Coufová, P.; Novák, J.; Hlasivcová, N. Hydroxyl as a Defect of the Perovskite BaTiO₃ Lattice. *J. Chem. Phys.* **1966**, *45*, 3171–3174. [CrossRef]
36. Cho, Y.J.; Nguyen, N.V.; Richter, C.A.; Ehrstein, J.R.; Lee, B.H.; Lee, J.C. Spectroscopic ellipsometry characterization of high-*k* dielectric HfO₂ thin films and the high-temperature annealing effects on their optical properties. *Appl. Phys. Lett.* **2002**, *80*, 1249–1251. [CrossRef]
37. Nam, T.; Park, Y.J.; Lee, H.; Oh, I.-K.; Ahn, J.-H.; Cho, S.M.; Kim, H.; Lee, H.-B.-R. A composite layer of atomic-layer-deposited Al₂O₃ and graphene for flexible moisture barrier. *Carbon N. Y.* **2017**, *116*, 553–561. [CrossRef]
38. Hu, B.; Yao, M.; Xiao, R.; Chen, J.; Yao, X. Optical properties of amorphous Al₂O₃ thin films prepared by a sol-gel process. *Ceram. Int.* **2014**, *40*, 14133–14139. [CrossRef]
39. Cheynet, M.C.; Pokrant, S.; Tichelaar, F.D.; Rouvière, J.-L. Crystal structure and band gap determination of HfO₂ thin films. *J. Appl. Phys.* **2007**, *101*, 054101. [CrossRef]
40. Liu, C.; Chor, E.F.; Tan, L.S. Enhanced device performance of AlGaN/GaN HEMTs using HfO₂ high-*k* dielectric for surface passivation and gate oxide. *Semicond. Sci. Technol.* **2007**, *22*, 522–527. [CrossRef]
41. Viezbicke, B.D.; Patel, S.; Davis, B.E.; Birnie, D.P. Evaluation of the Tauc method for optical absorption edge determination: ZnO thin films as a model system. *Phys. Status Solidi* **2015**, *252*, 1700–1710. [CrossRef]
42. Moreira, L.; Ponce, L.; De Posada, E.; Flores, T. Er:YAG polycrystalline ceramics: Use of SiO₂ and B₂O₃ as sintering additives and their effects on the optical and structural properties. *Rev. Cuba. Fis.* **2017**, *34*, 125–132.
43. Taouririt, T.E.; Meftah, A.; Sengouga, N. Effect of the interfacial (low-*k* SiO₂ vs high-*k* Al₂O₃) dielectrics on the electrical performance of a-ITZO TFT. *Appl. Nanosci.* **2018**, *8*, 1865–1875. [CrossRef]
44. Rahman, M.M.; Kim, J.-G.; Kim, D.-H.; Kim, T.-W. Characterization of Al Incorporation into HfO₂ Dielectric by Atomic Layer Deposition. *Micromachines* **2019**, *10*, 361. [CrossRef]
45. Zhou, L.; Lu, X.; Chen, L.; Ouyang, X.; Liu, B.; Xu, J.; Tang, H. Leakage Current by Poole–Frenkel Emission in Pt Schottky Contacts on () β-Ga₂O₃ Grown by Edge-Defined Film-Fed Growth. *Ecs J. Solid State Sci. Technol.* **2019**, *8*, Q3054–Q3057. [CrossRef]
46. Wang, Z. Detection of and Protection against Plasma Charging Damage in Modern IC Technology. Ph.D. Thesis, University of Twente, Enschede, The Netherlands, 2004.
47. Park, H.B.; Cho, M.; Park, J.; Hwang, C.S.; Lee, J.-C.; Oh, S.-J. Effects of plasma nitridation of Al₂O₃ interlayer on thermal stability, fixed charge density, and interfacial trap states of HfO₂ gate dielectric films grown by atomic layer deposition. *J. Appl. Phys.* **2003**, *94*, 1898–1903. [CrossRef]

